Refined effective-medium model for the optical properties of nanoparticles coated with anisotropic molecules

Chhayly Tang [*], Baptiste Auguié, and Eric C. Le Ru [†]

The MacDiarmid Institute for Advanced Materials and Nanotechnology, School of Chemical and Physical Sciences,
Victoria University of Wellington, P.O. Box 600, Wellington 6140, New Zealand

This work aims to provide a simple yet complete effective dielectric function for an anisotropic layer of polarizable molecules adsorbed on a metallic surface. This effective medium model considers the important and nontrivial case of nonvacuum embedding media and accounts for orientation effects, coverage dependence through dipole-dipole interactions, and image-dipole effects. To check the model's validity, we focus in particular on the experimentally relevant case of dyes adsorbed on metallic nanospheres. We can then use anisotropic Mie theory, together with the effective dielectric function describing the molecular coating, to calculate their optical properties. We show that this effective medium description is in very good agreement with more elaborate and computationally intensive microscopic calculations based on coupled-dipole models. The effective medium model therefore provides a simple means to investigate orientation effects and coverage dependence, including in more complex systems such as dyes adsorbed on nonspherical or ensembles of nanoparticles. This model can readily be used to further our theoretical understanding of dye-nanoparticle systems, for example in the context of dye-plasmon resonance coupling or surface-enhanced Raman and fluorescence spectroscopy.

I. INTRODUCTION

Interactions between surface plasmons in metallic nanoparticles and electronic resonance in adsorbates are central to many areas of research, including subwavelength manipulation (nanoantennas [1,2], or metamaterials [3,4]), surface-enhanced spectroscopy (Raman and fluorescence) [5–11], and plasmon-enhanced applications for solar cells [12,13]. Many recent studies have investigated experimentally and theoretically such interactions between the plasmon resonance of metallic films/nanoparticles and the optical resonance of dyes adsorbed on their surfaces [14–21], with a recent surge of interest in the strong-coupling regimes [22–24].

In these contexts, the optical properties of adsorbed molecular (sub)monolayers on nanoparticles have been mostly studied within classical electromagnetic theory. The most common type of models [14,18–20,25–28] are effective medium models (EMMs), where the discrete molecular layer is replaced by a thin continuous shell with an effective dielectric function [29–31]. The problem then reduces to solving Maxwell's equations for piecewise continuous media, which can be done using, for example, Mie theory [for spherical nanoparticles (NPs)] [19,20,26], Finite-Difference Time Domain (FDTD) modeling for more general shapes [23,24,32], or approximations such as the quasistatic approximation for spheroidal particles [14,26,27]. EMMs used to date have several limitations. In many instances, the effective dielectric

functions are phenomenological and not quantitative, lacking a direct link to microscopic parameters. Local field effects, i.e., the effects of the field created by one molecule on the others, have seldom been considered, which restricts the validity to low surface coverage. Any anisotropy expected from a preferential molecular orientation on the surface is also usually neglected. Despite these many limitations, these models are still routinely used because of their relative simplicity.

The alternative approach and most refined model to date consists of a microscopic approach where each molecule is treated as a polarizable dipole and the self-consistent field created by the mutual interaction of all molecules is calculated, a method called coupled dipole model (CDM) [33]. The solution is mathematically similar to the commonly used discrete dipole approximation [34,35]. The CDM was recently applied to molecular dipoles arranged in a spherical shell geometry to elucidate the effect of dye-dye interactions [36] on the optical properties in a nonplanar arrangement. For molecules adsorbed on a NP, it is possible to extend the CDM to include the effect of the core NP, by solving Maxwell's equations for the interaction between each dipole and the nanoparticle, an extension which we will refer to below as NP-CDM. This approach was recently implemented for spherical NPs using Mie theory to investigate the electromagnetic interactions of dye molecules adsorbed onto a nanosphere [37]. It can be used to study a rich array of interrelated parameters that influence the optical properties: molecular orientation, dye-dye interactions, self-reflected field or image-dipole effect, and spatial distribution of adsorbates. However, the main shortcoming of the NP-CDM is the computing requirements, even for the simple case of spheres where Mie theory provides a fast and efficient solution. Modeling a 60-nm-diameter

[*]chhayly.tang@vuw.ac.nz
[†]eric.leru@vuw.ac.nz

nanosphere with a 1 nm^{-2} coverage of adsorbate requires more than 10^4 polarizable dipoles. To give an order of magnitude, computing a spectrum (100 wavelength points) may then take from a few hours to a day on a high-end PC, which prevents systematic multiparameter studies. NP-CDM is also limited to spherical nanoparticles at this stage. It is worth emphasizing in this context that the NP-CDM is different from previous schemes where the response of the NP is approximated as dipolar. In this approximation, the solution is a standard CDM problem and nonspherical NP or multiple NPs can easily be implemented efficiently. The NP-CDM is much more advanced as it accounts for the NP response exactly (solving Maxwell's equation for a dipole next to the NP). This extra refinement is required when molecules are close to the NP surface, as in most cases of interest in plasmonics. NP-CDM is challenging even for spheres as it requires including multipolar orders typically up to 500 [37]. It could, in principle, be implemented for other shapes and multiple particles, for example using the T-matrix framework, but would likely run into numerical problems at high multipole orders [38] and fundamental problems related to the Rayleigh hypothesis [39].

The aim of this work is to develop and validate an improved effective medium model with comparable predictive power as the NP-CDM, but without the high computational cost and complexity. This model is moreover applicable to general nanoparticle shapes when combined with numerical Maxwell's equations solvers. To achieve this goal, we combine and extend a number of concepts that have been previously developed in isolation into a complete EMM. Effective dielectric functions for a two-dimensional (2D) anisotropic medium have already been derived in the context of 2D planar arrays of dipoles by Dignam and Moskovits [40] and further developed by Bagchi *et al.* [41,42] to include image-dipole effects. We will show that the latter improvement is indeed necessary to reproduce the NP-CDM predictions. These previous models were applied only to planar arrays adsorbed on planar films; we will here investigate their application to nanoparticles, where the anisotropic layer wraps around a curved surface. Another crucial aspect we consider is the embedding medium surrounding the molecules and particles; all previous works were carried out for dipoles/molecules in vacuum. We here generalize the 2D anisotropic effective dielectric function to an isotropic embedding medium with permittivity $\varepsilon_m \neq 1$, which is relevant to many experimental conditions where particles are suspended in water or other solvents. As we will show, this generalization is not straightforward as it requires one to appropriately include local field effects related to the solvent molecules. We discuss our results in the special case of dyes adsorbed on a metallic nanosphere, which can be directly compared with the benchmark predictions from the NP-CDM [37]. For this, we use the full solution of anisotropic Mie scattering by an isotropic core/anisotropic shell system derived by Roth and Dignam [43]. We show that in some circumstances, the EMM with a single shell immediately adjacent to the core does not adequately reproduce NP-CDM results and introduce a two-layer model to overcome this discrepancy. This two-layer model moreover lends itself to further simplification in the
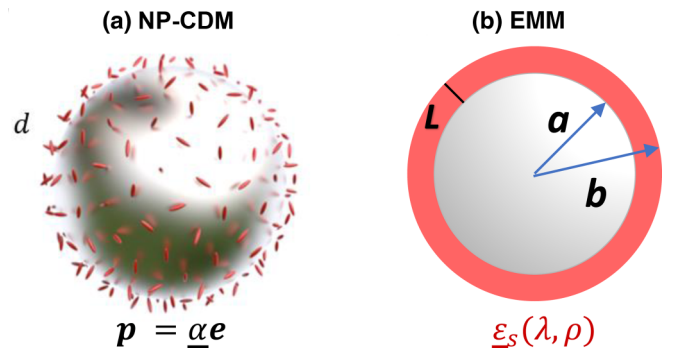
FIG. 1. (a) Schematics of discrete polarizable dipoles adsorbed onto a nanoparticle at a distance d from the surface. The elongated ellipsoids represent a uniaxial polarizability tensor, here with random orientation. (b) Corresponding effective medium model where the dipoles are replaced by a continuous shell of thickness L and dielectric function $\underline{\varepsilon}_s$, possibly tensorial.

thin-shell approximation along the lines of previous work [44].

II. PRELIMINARIES

A. Model system

We consider a monolayer or submonolayer coverage of adsorbates on a nanoparticle, here a nanosphere of radius a, as depicted in Fig. 1(a). The coverage or surface concentration is characterized by the number of molecules per surface area, ρ. They are assumed to be adsorbed at a fixed distance d from the surface and the number of molecules is therefore $N = 4\pi(a + d)^2\rho$. This is a common assumption, which can be justified for chemically adsorbed molecules where the adsorption geometry is well defined, or for physisorbed molecules in the presence of a well-defined coating layer on the metal surface. We assume that the optical response of the molecules is known and described by a vacuum dipolar polarizability tensor $\underline{\alpha}$: the microscopic electric field $\mathbf{e}$ at a molecule position induces a dipole $\mathbf{p} = \underline{\alpha}\mathbf{e}$. Each dipole, including those comprising the solvent, then creates a field, which adds to the incident field and the field scattered by the nanoparticle to give the microscopic field at each molecule position. The exact solution for these self-consistent interactions can be found within the generalized coupled-dipole model (NP-CDM) approach in the special case of a spherical nanoparticle [37].

To benchmark our EMM predictions against NP-CDM, we choose to focus on the specific example of a silver sphere of radius $a = 14$ nm, with a core dielectric function ε_c as given in Ref. [6], and embedded in water with dielectric function $\varepsilon_m = (1.33)^2$. This sphere radius is large enough to avoid strong curvature effects, and small enough to allow for NP-CDM calculations to be carried out in a reasonable time. The adsorbate is chosen to be a uniaxial dye with a single Lorentzian resonance at 526 nm. Many dyes have a preferred axis associated with their electronic absorption (along which the electrons are most delocalized, typically along the aromatic rings). The assumption of uniaxial polarizability is therefore often justified, especially close to the resonance. Explicitly the dye polarizability tensor is therefore of the form

$\begin{pmatrix} 0 & 0 & 0 \\ 0 & 0 & 0 \\ 0 & 0 & \alpha_{\text{uni}} \end{pmatrix}$) when written in the molecular axes with

$$\alpha_{\text{uni}}(\lambda) = \alpha_\infty + \frac{\alpha_1 \lambda_1}{\mu_1} \left[\frac{1}{1 - \frac{\lambda_1^2}{\lambda^2} + i \frac{\lambda_1^2}{\lambda \mu_1}} - 1 \right], \quad (1)$$

where $\alpha_\infty = 9.6 \times 10^{-39}$ [SI], $\alpha_1 = 5.76 \times 10^{-38}$ [SI], $\lambda_1 = 526$ nm, and $\mu_1 = 10^4$ nm. This is a simple Lorentz oscillator model with parameters matching the experimentally measured optical properties of the main absorption peak of rhodamine 6G [45]. The optical response of this dye/NP system is dominated by the silver NP absorption and scattering, especially at low dye concentrations. In order to identify more clearly the effect of the dye layer, we will therefore consider the differential absorption cross section δC_{abs}, which we define as the difference between the absorption cross section of the full system (NP+dye) and that of the bare NP, obtained in a separate simulation. For plotting purposes, this will be normalized to the number of adsorbates, namely, $\delta C_{\text{abs}}/N$, which can then be directly compared to the isolated adsorbate absorption cross section, as done in Refs. [21,36,37].

B. Molecular orientation

In effective medium models, [30,31] one replaces the discrete dipole layer by a homogeneous shell of thickness L and effective dielectric tensor $\underline{\varepsilon}_s$ [Fig. 1(b)]. To derive $\underline{\varepsilon}_s$ rigorously, further assumptions must be made on the adsorbate orientations, for example random orientation as illustrated in Fig. 1(a). In order to match the symmetry of the problem, the effective dielectric tensor is usually taken as diagonal in the spherical basis, with ε_n and ε_t its components along the normal and tangent to the NP surface. Two cases particularly relevant to experiments are when the molecular axis is perpendicular ($\perp$) or tangential ($\parallel$) to the surface. The corresponding polarizability tensor for perpendicular orientation is simply

$$\underline{\alpha}_d^\perp = \begin{pmatrix} 0 & 0 & 0 \\ 0 & 0 & 0 \\ 0 & 0 & \alpha_{\text{uni}} \end{pmatrix} \quad (2)$$

in the local basis $(\hat{\mathbf{x}}', \hat{\mathbf{y}}', \hat{\mathbf{z}}')$ where $\hat{\mathbf{z}}'$ denotes the normal to the surface (for a sphere, this is the spherical basis up to reordering, i.e., $\hat{\mathbf{z}}' \equiv \hat{\mathbf{r}}$). For tangential orientation, orientation averaging is still necessary and for simplicity, we will assume an effective polarizability tensor that is isotropic in the plane:

$$\underline{\alpha}_d^\parallel = \begin{pmatrix} \alpha_{\text{uni}}/2 & 0 & 0 \\ 0 & \alpha_{\text{uni}}/2 & 0 \\ 0 & 0 & 0 \end{pmatrix}. \quad (3)$$

The effective dielectric tensor $\underline{\varepsilon}_s$ is expected to have the same symmetry property as these polarizability tensors, if no spatial ordering of the adsorbed species introduces additional asymmetries. A square or a random lattice both satisfy this criterion (note, however, that the square lattice is an idealization as the adsorbates will rarely form a perfect crystal).

C. Mie theory

To predict optical properties using the EMM, we solve the scattering problem for an anisotropic shell of dielectric tensor $\underline{\varepsilon}_s$ surrounding an isotropic core (radius a and dielectric function ε_c) embedded in a medium with ε_m. For this, we use the general solution of Mie theory for an anisotropic shell developed in Ref. [43]. The solution has many similarities with Mie theory, with some complications associated with the use of spherical Bessel functions of complex order (i.e., j_w and y_w with w a complex number instead of an integer as in standard Mie theory).

The derived Mie scattering coefficients are functions of the relative indices of refraction, $s_c = \sqrt{\varepsilon_c}/\sqrt{\varepsilon_m}$ and $s_t = \sqrt{\varepsilon_t}/\sqrt{\varepsilon_m}$, the dielectric function for the normal direction, ε_n, and the size parameters $x = k_m(a + L) = k_m b$ and $y = k_m a$, where $k_m = 2\pi\sqrt{\varepsilon_m}/\lambda$. From them, the optical properties, such as scattering, extinction, and absorption spectra can be derived as in standard Mie theory. The isotropic Mie theory solution for the core only is then subtracted to derive the corresponding differential cross sections characterizing the effect of the dye layer.

We have used a relatively small number ($N_{\text{max}} = 5$) of multipoles for all anisotropic Mie theory calculations. One can check that the results are in fact almost converged when including only $N_{\text{max}} = 1$ (the dipole terms) in the cases we studied. This is in stark contrast with NP-CDM calculations, where dipole-sphere interactions typically require $N_{\text{max}} = 500$ to properly account for image-dipole effects [37]. For the small sphere size considered here, one could also use the electrostatic solution as an approximate solution, but the accuracy is not very good even at a radius of 14 nm [46], and in any case Mie theory allows for straightforward generalization to larger spheres.

III. EFFECTIVE MEDIUM MODELS FOR MOLECULAR MONOLAYERS

A. Isotropic EMM

In many previous studies [14,18–20,25–28], $\underline{\varepsilon}_s$ is taken isotropic, $\underline{\varepsilon}_s = \varepsilon_s \underline{I}$, and constructed empirically using one or more Lorentz oscillators accounting for the molecular resonance(s). This approach, however, loses the quantitative connection between ε_s and the adsorbate concentration ρ. A more rigorous approach is to express ε_s in terms of the microscopic properties, i.e., $\underline{\alpha}$. For randomly oriented molecules distributed uniformly in vacuum, we simply have in the dilute regime (small ρ) [29,47]

$$\varepsilon_s \approx 1 + 3\bar{\alpha}_d, \quad \text{with} \quad \bar{\alpha}_d = c_d \frac{\text{Tr}(\underline{\alpha})/3}{\varepsilon_0}, \quad (4)$$

where $\text{Tr}(\underline{\alpha})/3$ accounts for the orientation averaging. c_d is the adsorbate volumic concentration in the shell:

$$c_d = \frac{3N}{4\pi(b^3 - a^3)} \approx \frac{\rho}{L}, \quad (5)$$

the latter approximation assuming $L, d \ll a$. We note that the thickness of the effective medium shell, L, has not been specified and does not necessarily correspond to a physical quantity such as the thickness of the monolayer or the distance d of the adsorbate from the surface. In fact, although ε_s depends on L, the predicted optical properties do not in the limit of small L, as illustrated in Fig. 2(a). This can be understood in simple terms as the shell absorption is in a first approximation
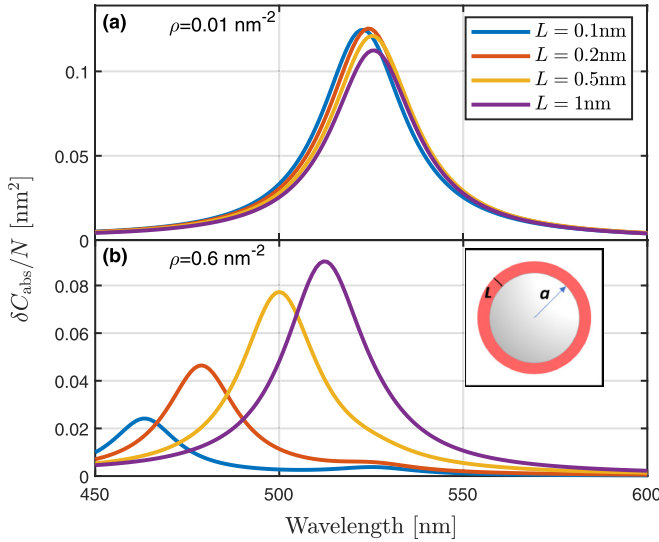
FIG. 2. Shell-thickness (L) dependence of the differential absorption cross section for an isotropic EMM for (a) the dilute regime ($\rho = 0.01$ nm^{-2}) where ε_s is defined by Eq. (4), and (b) high coverage ($\rho = 0.6$ nm^{-2}), using Eq. (6) instead. A strong L dependence is observed in the latter case. The silver sphere radius is $a = 14$ nm.

proportional both to the shell volume, itself proportional to L, and to Im(ε_s), which is proportional to $1/L$ from Eqs. (4) and (5).

At increased coverage, the interactions between molecules result in local field effects, which can be included using the Clausius Mossotti [29,31] relation (also known as Lorentz-Lorenz relation) and its inverse:

$$\varepsilon_s = \frac{1 + 2\bar{\alpha}_d}{1 - \bar{\alpha}_d}, \quad \bar{\alpha}_d = \frac{\varepsilon_s - 1}{\varepsilon_s + 2}. \tag{6}$$

This introduces a nonlinear dependence of ε_s on ρ, but also on L. The predictions then become strongly dependent on L [see, for example, Fig. 1(b)]. In effect, reducing L increases the effective concentration and the interaction between molecules even if the coverage ρ is unchanged, which is unphysical. In order to make predictions, L must therefore be fixed using theoretical arguments, for example the approach proposed by Dignam and Moskovits [40], which gives $L = 0.935\rho^{-1/2}$. We note that in the form presented above, this EMM does not allow for an embedding medium with a nonunity refractive index like water, but this aspect can be addressed as in Ref. [21].

This isotropic EMM has been used in many occasions, but fails to account for molecular orientation or image-dipole effects, and misrepresents dipole-dipole interactions if L is not chosen carefully. An anisotropic model is desirable as it is well accepted that the adsorption orientation of molecules adsorbed on metallic nanoparticles can significantly affect the optical properties of the system, for example in the context of surface selection rules in surface-enhanced Raman spectroscopy [6,48–50]. Image-dipole effects are also predicted to play an important role for molecules close to a metal surface [37].

B. Anisotropic EMM in vacuum

To overcome these shortcomings, we draw from previous studies of adsorbed monolayers on flat surfaces in the context of ellipsometry [40,51,52] or differential reflectance spectroscopy [41,42]. For a 2D array of isotropic polarizable dipoles of polarizability α in vacuum, at a distance d from a semi-infinite material with dielectric function ε_c, it was shown that the effective dielectric function for in-plane excitation is

$$\varepsilon_{xy} = 1 + \frac{\frac{c_d \alpha}{\varepsilon_0}}{1 - \frac{\alpha}{8\pi\varepsilon_0}\rho^{3/2}(\xi_0 + \beta\xi_I)}, \tag{7}$$

and for out-of-plane excitation:

$$\frac{1}{\varepsilon_z} = 1 - \frac{\frac{c_d \alpha}{\varepsilon_0}}{1 + \frac{\alpha}{4\pi\varepsilon_0}\rho^{3/2}(\xi_0 - \beta\xi_I)}. \tag{8}$$

c_d is again the volumic dipole concentration in the layer, and ξ_0 is a lattice sum on the (normalized) molecule positions, which has been calculated in the case of an infinite square lattice [53]. The sum is slowly convergent but can be recast as a fast converging series [52,54] to obtain its numerical value, sometimes called the Topping constant:

$$\xi_0 = \sum_{n,k \neq (0,0)}^{\infty} \frac{1}{(n^2 + k^2)^{3/2}} \approx 9.033\,565. \tag{9}$$

The term $\beta\xi_I$ in Eqs. (7) and (8) is related to the image-dipole effect [41,42] and is only important for small distance d of the dipole to the surface (typically less than 1 nm in cases of interest). Explicitly, we have

$$\beta = \frac{\varepsilon_c - 1}{\varepsilon_c + 1} \tag{10}$$

and

$$\xi_I = \sum_{n,k=-\infty}^{\infty} \frac{8\rho d^2 - (n^2 + k^2)}{[n^2 + k^2 + 4\rho d^2]^{5/2}}. \tag{11}$$

ξ_I is akin to a lattice sum like ξ_0 but note that it depends on d and ρ. It can be computed more efficiently through the equivalent sum [42]

$$\xi_I = 16\pi^2 \sum_{n=0}^{\infty} \sum_{k=1}^{\infty} \sqrt{n^2 + k^2} \exp[-4\pi d\sqrt{\rho}\sqrt{n^2 + k^2}]. \tag{12}$$

We note that this approach is similar in essence to the microscopic CDM. Here we first consider static point dipoles in an infinite square lattice, calculating their self-consistent interaction to embed them into an effective macroscopic dielectric function. In contrast the CDM maintains the explicit pairwise retarded interaction between all the dipoles in the final geometry of interest. For spherical arrangements, agreement between the two methods presupposes that the effect of the layer's curvature on the dipole-dipole interactions is negligible, which is expected to hold for core particles with a sufficiently large radius of curvature.

C. Anisotropic EMM in a medium

Before applying and validating these expressions, we first generalize them to the much more experimentally relevant

case of $\varepsilon_m \neq 1$, for example for molecules embedded in water. Despite its importance, we could not find any generalization in the literature, and in fact it does not appear to be straightforward. In a medium, we now need to take into account the local field effects of the medium molecules onto the adsorbate [6,55,56]. For the coverages considered here, up to ~ 1 nm^{-2}, the solvent (e.g., water) molecules remain the dominant species even in the adsorbed molecular layer. We therefore choose to treat the embedding medium macroscopically, i.e., as a continuum medium in which the polarizable dipoles are embedded. A different approach may be needed at very high dipole coverages (where water molecules may no longer be dominant in the dipole layer) [29]. Within this mixed microscopic/continuum approach, we can show that Eqs. (7) and (8) generalize to

$$\varepsilon_{xy} = \varepsilon_m + \frac{L_m^2 \frac{c_d \alpha}{\varepsilon_0}}{1 - \frac{\alpha}{8\pi\varepsilon_0}\frac{L_m^2}{\varepsilon_m}\rho^{3/2}(\xi_0 + \beta_m \xi_I)}, \quad (13)$$

$$\frac{1}{\varepsilon_z} = \frac{1}{\varepsilon_m} - \frac{\frac{L_m^2}{\varepsilon_m^2}\frac{c_d \alpha}{\varepsilon_0}}{1 + \frac{\alpha}{4\pi\varepsilon_0}\frac{L_m^2}{\varepsilon_m}\rho^{3/2}(\xi_0 - \beta_m \xi_I)}, \quad (14)$$

where

$$\beta_m = \frac{\varepsilon_c - \varepsilon_m}{\varepsilon_c + \varepsilon_m} \quad (15)$$

and

$$L_m = (\varepsilon_m + 2)/3 \quad (16)$$

is the microscopic local field correction factor [6,55,56]. This factor accounts for local field corrections due to the solvent molecules, which are assumed to be the dominant species and uniformly distributed in space. In this case, the microscopic field at the molecule position, **e**, is related to the macroscopic field **E** obtained from solving Maxwell's equations by $\mathbf{e} = L_m \mathbf{E}$. By optical reciprocity, this scaling factor also applies to the field created by a dipole embedded in the same medium, hence the factors L_m^2 appearing in the expressions above. More details on the derivations are given in Appendix A.

To validate the EMM against the microscopic CDM, we consider, in particular, the two cases introduced earlier in Fig. 1: radially oriented ($\perp$) and tangentially oriented with in-plane isotropy ($\parallel$) molecules. To implement the anisotropic EMM, we then set

$$\varepsilon_n^\perp = \varepsilon_z, \quad \varepsilon_t^\perp = \varepsilon_m, \quad \alpha = \alpha_{\text{uni}} \quad (17)$$

for the first case and

$$\varepsilon_n^\parallel = \varepsilon_m, \quad \varepsilon_t^\parallel = \varepsilon_{xy}, \quad \alpha = \alpha_{\text{uni}}/2 \quad (18)$$

for the second. Although not our focus here, it is worth pointing out that this anisotropic EMM is also relevant to molecules with a fully isotropic response (or randomly oriented molecules). The 2D arrangement breaks the symmetry of the molecular response and an anisotropic dielectric function is still required:

$$\varepsilon_n^{\text{iso}} = \varepsilon_z, \quad \varepsilon_t^{\text{iso}} = \varepsilon_{xy}, \quad \alpha = \alpha_{\text{uni}}/3. \quad (19)$$

We will not consider intermediate orientations here, corresponding, for example, to a molecule adsorbing with its main axis at a fixed angle β to the surface normal, but it can, in

principle, also be modeled within the same EMM as follows. Equations (2) and (3) can be generalized to

$$\underline{\alpha}_d = \cos^2\beta \, \underline{\alpha}_d^\perp + \sin^2\beta \, \underline{\alpha}_d^\parallel. \quad (20)$$

In principle, this tensor also has off-diagonal terms, but they do not have any influence in the derivation of the effective medium model because in a planar arrangement, a dipole along x (respectively, z) does not induce an electric field along z (respectively, x) at the other dipole positions. This therefore translates to an effective dielectric tensor given by

$$\begin{aligned} \varepsilon_n^\perp &= \varepsilon_z \quad \text{with} \quad \alpha = (\cos^2\beta)\alpha_{\text{uni}}, \\ \varepsilon_t^\perp &= \varepsilon_{xy} \quad \text{with} \quad \alpha = (\sin^2\beta)\alpha_{\text{uni}}/2. \end{aligned}$$

Let us now consider planar and spherical dipole arrangements in water (i.e., no metal surface or nanoparticle). The anisotropic EMM results can then be directly compared to CDM calculations, as summarized in Fig. 3. The EMM problem is solved for a planar interface using a simple generalization of Fresnel equations to such anisotropic media [57]. We consider for illustration the specific case of 45° incidence with p polarization, as it presents electric field components both perpendicular and parallel to the plane of dipoles. Other cases result in the same conclusions. As shown in Figs. 3(a)–3(c) the EMM predictions are then indistinguishable from the analytic microscopic model for a 2D planar array of molecules in water, which can be derived following Ref. [58] as discussed in Appendix A. In the special case of isotropic molecules [Fig. 3(c)], the anisotropic EMM works much better than the full isotropic solution based on Clausius Mosotti relations [Eq. (6)] generalized to $\varepsilon_m \neq 1$, where molecules are assumed to be arranged in a homogeneous three-dimensional (3D) configuration (in a cubic or disordered lattice, as per the standard derivations). We conclude that this anisotropic EMM performs extremely well on flat surfaces. While this may seem trivial, in that both models were derived by considering an infinite lattice of dipoles, it is interesting to note that the Fresnel model of the effective medium layer considers retardation effects very differently from the retardation in the lattice sum of the microscopic CDM.

We then consider the model's applicability to a spherical shell of molecules embedded in water and solve the equivalent EMM with radially anisotropic Mie theory. This is equivalent to wrapping the 2D planar sheet around a sphere, as depicted in Fig. 3(g). As long as the radius of the core particle is large enough, the dipole-dipole interactions should be dominated by near neighbors in a locally quasiplanar configuration and the EMM predictions should be correct. As shown in Figs. 3(d)–3(f), the EMM predictions are indeed very close to the microscopic solution obtained from a coupled dipole model [36]. At large coverage, there is a small discrepancy for the parallel case [Fig. 3(f)], which becomes more prominent for smaller sphere radius (not shown here) and is therefore attributed to a small curvature effect. But overall it appears that the 2D plane anisotropic effective dielectric functions can be applied to spherical shells embedded in water.
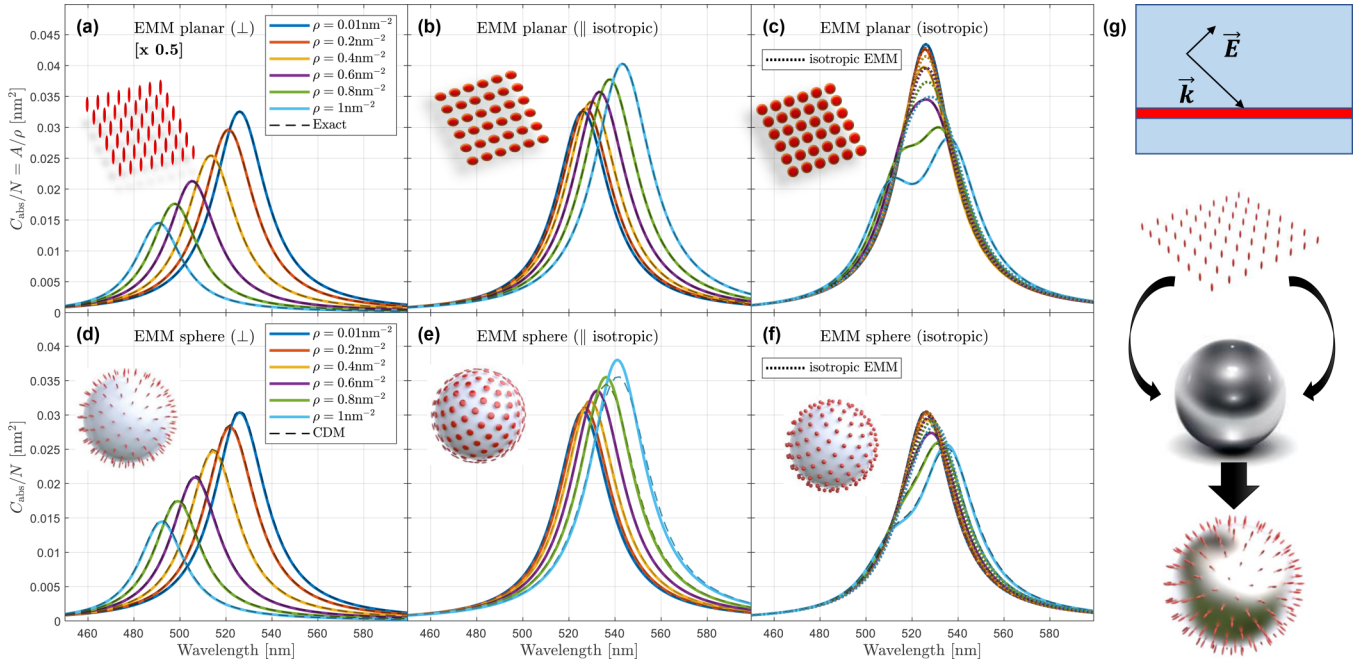
FIG. 3. (a)–(c) Anisotropic-EMM predictions for the absorption spectrum of an $L = 1$-nm-thick planar layer of perpendicular (a), in-plane isotropic (b), or fully isotropic (c) dipoles in water compared to the analytic solutions of a 2D array of dipole given in Appendix A (dashed lines). The agreement is excellent. The isotropic-EMM model is also shown as a dotted line in (c). For spherical arrangement of molecules, the same anisotropic EMM is used, as shown schematically in (g). (d)–(f) The predictions for spherical shells in water are compared to microscopic coupled-dipole models (dashed line) for perpendicular (d), in-plane (e), and isotropic (f) arrangements. The inner radius of the water sphere is 14 nm. Different coverages ρ are considered in all cases. Equations (17)–(19) are used for the anisotropic EMM with $d = 1$ nm (but the image-dipole effect is negligible and could also be ignored in this case as there is no metal).

IV. APPLICATION OF THE EFFECTIVE MEDIUM MODEL TO SPHERICAL NANOPARTICLES

We now discuss the validity and applicability of the derived anisotropic EMM/Mie theory predictions for dyes adsorbed on a metallic nanoparticle by comparing them to those of NP-CDM.

A. Effective shell thickness

We first study in Fig. 4 the effect of the effective medium shell thickness L for dipoles at a distance $d = 1$ nm (large enough to avoid image-dipole effects for the moment). An intermediate coverage of $\rho = 0.6$ nm^{-2} is chosen to ensure dye/dye interactions effects are non-negligible, which results in a small blueshift ($\perp$ case) or redshift ($\parallel$ case) of the absorption, but the conclusions are independent of coverage. The effective dielectric functions have a similar L dependence as in the dilute isotropic case, $(\varepsilon_s - \varepsilon_m) \sim 1/L$, so one would expect that the results are not L dependent, at least for small L. This is indeed the case when considering a spherical layer of dye suspended in water [Figs. 4(a) and 4(d)]. However, for dyes adsorbed on a silver sphere, a relatively strong L dependence is observed even for small L [Figs. 4(b) and 4(e)]. This can be attributed to the large field intensity gradients close to the surface of the nanosphere (see Appendix B). The surface-averaged radial field intensity drops by 28% by moving only 1 nm away from the surface. Because the absorption in the effective layer scales with the field intensity, the average absorption over the full layer will decrease as the shell

becomes thicker, as observed in Figs. 4(b) and 4(e). The drop of surface-averaged field intensity as a function of distance is even more dramatic for the tangential component (62% at 1 nm), which explains the more pronounced L dependence for parallel molecules [Fig. 4(e)].

For a microscopic submonolayer of molecules, the field that matters is the field at the molecule positions (a distance d from the surface). By choosing an effective medium thickness of $L = 2d$, we should therefore obtain a good approximation of the NP-DCM results. This is indeed the case as seen in Figs. 4(b) and 4(e), although the agreement is not perfect in the parallel case because the drop in field intensity is not linear over this range (see Appendix B). To overcome this issue, we propose instead a two-layer effective medium shell model as shown schematically in the inset of Fig. 4(c). The core is surrounded by a water (or air) layer of thickness $d - L/2$, i.e., the effective medium shell is centered at the dipole positions (distance d from the surface) while remaining as thin as desired (L small). The resulting EMM predictions are then in perfect agreement with NP-CDM for small L [Figs. 4(c) and 4(f)], and this approach therefore removes any ambiguity in the choice of L. Arguably, the one-layer EMM with $L = 2d$ was already pretty good, but one additional advantage of the two-layer EMM is that one can choose L very small and use the small shell thickness approximation to solve the problem. As discussed in Ref. [44], this dramatically simplifies the numerical computations, as Bessel functions of complex orders are no longer necessary. To implement this approach, the results of Ref. [44] must be extended to a two-layer system.
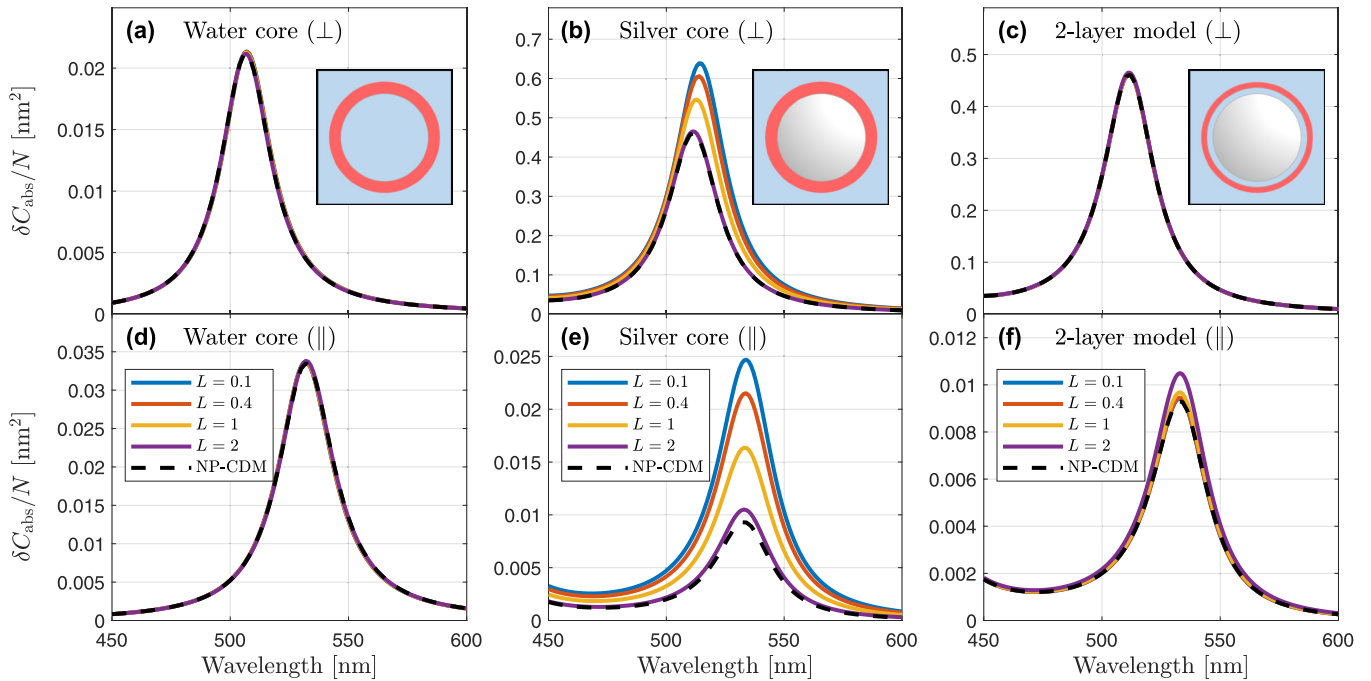
FIG. 4. Shell-thickness (L) dependence of the differential absorption cross section for an anisotropic EMM of a spherical layer of perpendicular (top) and parallel (bottom) adsorbates in water (a),(d) or around a silver sphere (b),(e). The latter case shows an undesirable L dependence, which can be avoided using an improved two-layer configuration (c),(f), where the effective shell layer is separated from the sphere surface by a distance $d - L/2$. In all cases, the core has radius $a = 14$ nm and a coverage of $\rho = 0.6$ nm^{-2} is used, but similar conclusions are obtained at other coverages. The results are compared to CDM and NP-CDM predictions for dipoles at a distance $d = 1$ nm from the water (fictitious) or silver core.

This simplification is rather technical and outside the scope of this work so will be presented elsewhere.

B. Image-dipole effect

When a polarizable dipole is located close to a dielectric or metallic surface/object, the electromagnetic field reflected (or scattered) by the object can affect its optical properties [6,59]. In a first approximation, for sufficiently small distance d the surface may be assumed to be planar and the retardation effects may be neglected, which results in a simple electrostatic problem with an analytic solution provided by the image-dipole method [6,47,60]. The main consequence of this interaction with the reflected field results is a modification of the dipole polarizability. For molecules excited in the visible and adsorbed on silver, this results in an orientation-dependent redshift of the dipole absorption for the smallest distances, typically under 1 nm, with a very strong distance dependence. This so-called image-dipole effect is rarely considered in studies of dye molecules on metals, but it has been shown to play a major role at distances smaller than 1 nm [37]. Moreover, for ensembles of dipoles, the reflected/scattered field will not only affect the dipole but also its neighbors and all the other dipoles. Such complex interactions cannot be modeled within the simple electrostatic model, but are accounted for within the NP-CDM [37]. The effective shell model we propose can also account for these multiple interactions [41,42].

This is first demonstrated in Fig. 5 for low coverage ($\rho = 0.01$ nm^{-2}) where the EMM results can be compared to the NP-CDM for a single dipole. The EMM predicts the correct
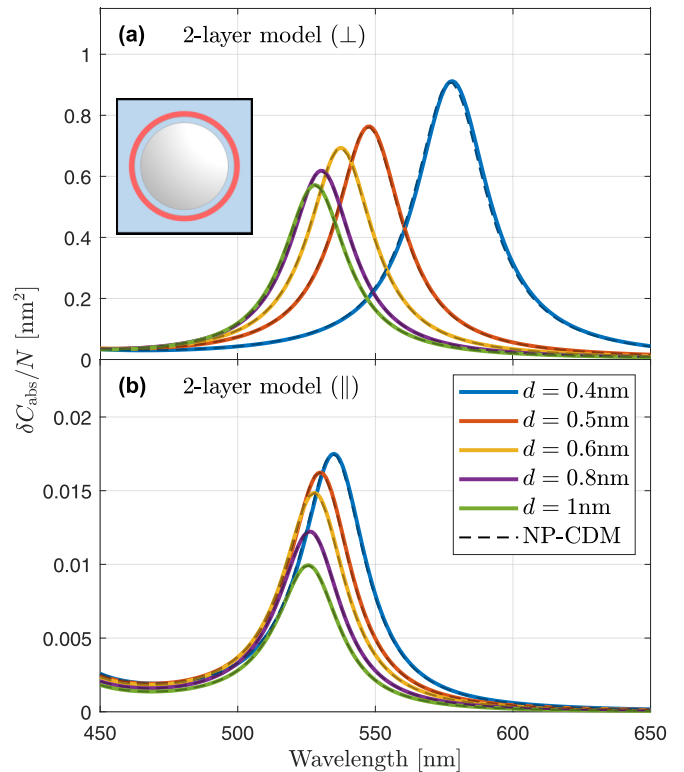
FIG. 5. Comparison between the EMM model and NP-CDM at low coverage $\rho = 0.01$ nm^{-2} for perpendicular (a) and parallel (b) orientations, for varying dipole distance from the surface, d. We here use the two-layer model with a small $L = 0.2$ nm.
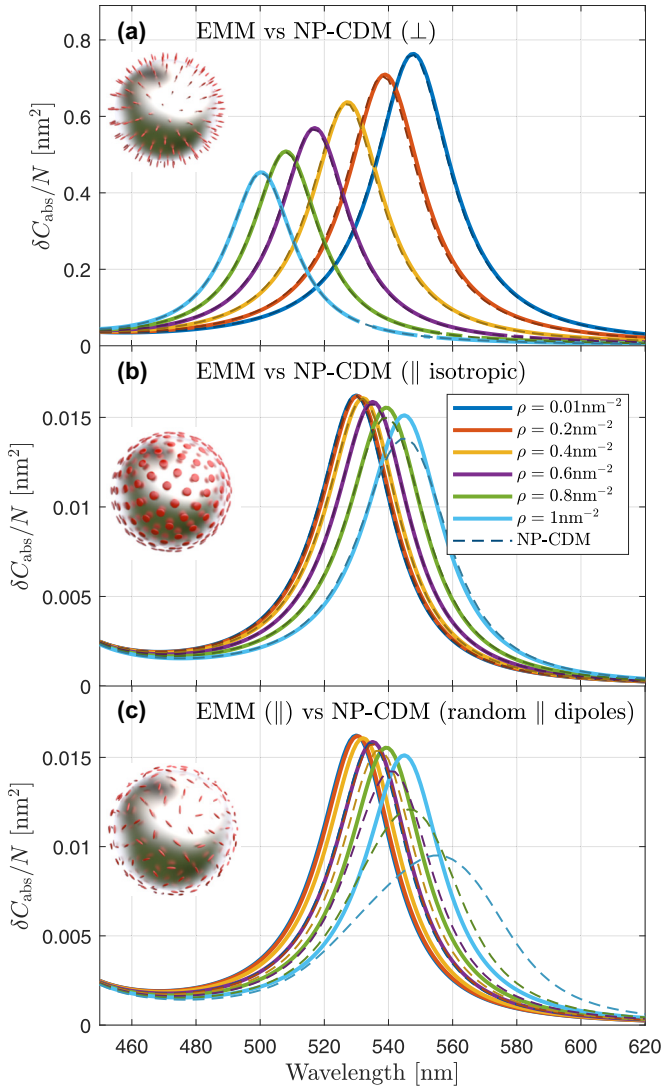
FIG. 6. Comparison between the two-layer EMM model and NP-CDM at a dipole distance where image-dipole effects are important, $d = 0.5$ nm, as a function of coverage for perpendicular (a) and parallel (b) orientations, for varying dipole distance from the surface, d. We use $L = 0.1$ nm and the thickness of the spacer water layer is $d - L/2$. In (c) the parallel EMM model [same as in (b)] is instead compared to NP-CDM for randomly oriented uniaxial dipoles.

redshift in absorption as a function of d for each orientation. The parameter d is here even more important as it determines the strength of the image-dipole-induced shifts, in addition to the secondary effect of the field intensity dependence discussed earlier. The two-layer model again allows us to choose L independently of d.

The effect of coverage is assessed in Fig. 6 for a fixed $d = 0.5$ nm. This distance is small enough to ensure that the image-dipole effects are not negligible, and we expect to observe the additional effect of the dipole/dipole interactions, including those mediated by the sphere [37]. It is therefore the most complex case. Again the proposed EMM performs very well: the agreement is extremely good for perpendicular orientation [Fig. 6(a)]. For parallel orientation [Fig. 6(b)], the EMM model predicts the correct absorption shift, but shows a

slight discrepancy in the intensity and width of the absorption peak at the highest coverages. A similar effect was already observed for spherical shells in water (Fig. 3) and attributed to a small curvature effect, which would therefore become less prominent for larger spheres. Finally, we compare in Fig. 6(c) the EMM predictions to those of the NP-CDM for randomly oriented in-plane dipoles. The discrepancy is larger in this case. The EMM does not account for the random in-plane orientation and instead replaces all dipoles by in-plane-isotropic polarizable elements (represented by oblate spheroids in our figures). Therefore, the information about the dipoles pointing in different (random) directions is lost, since the interaction between two uniaxial dipoles in random directions is not the same as the interaction between two isotropic dipoles. This point is further discussed and illustrated explicitly in Appendix C. The NP-CDM, which accounts for the orientation of all individual dipoles, provides a more realistic description, with the additional orientational disorder resulting, not unexpectedly, in a broadening of the absorption peak.

We note, however, that the optical response of molecules on metal surfaces is typically dominated by the perpendicular component, as evident in all our figures where the differential absorption spectra are much larger than for in-plane orientation. Therefore, the small errors observed between the EMM and the NP-CDM will in general have no effect for intermediate orientations where even a small perpendicular component would dominate.

V. CONCLUSION

We have introduced an effective medium model for molecular monolayers on a metallic surface that accounts for (i) nonvacuum embedding media, (ii) coverage dependence, (iii) molecular orientation effects, and (iv) image-dipole effects important at small separation from the surface. All these effects are relevant to typical experiments, for example dyes-on-nanoparticles. These effective dielectric functions were implemented into anisotropic Mie theory and compared to more elaborate predictions from a microscopic model to assess their validity and applicability. Good agreement was evidenced, which was further improved by considering a two-layer model with an ultrathin effective medium shell separated from the nanoparticle. This comparison was focused on the more commonly studied far-field properties, but we believe the EMM could also prove useful for near-field properties, which will be the subject of a follow-up study.

We believe that this anisotropic EMM will find application in many areas exploiting the optical properties of dyes on metallic nanoparticles, including molecular plasmonics (both weak- and strong-coupling regimes) and surface-enhanced spectroscopies, where the orientation, coverage, and distance to the surface of the adsorbates can have large effects. This work will, for example, facilitate the disentanglement of the various mechanisms at play in strong-coupling experiments from intrinsic shifts in electronic absorption, through dye-dye interactions, to plasmon-dye interactions. This model could also provide the basis for further theoretical studies of similar systems with nonspherical nanoparticles and/or assemblies of such particles, especially given that no NP-CDM implementation currently exists for these more complex systems.

APPENDIX A: ANALYTIC RESULTS FOR A PLANAR 2D LAYER OF DIPOLES

Reference [58] has derived analytic expressions for a 2D planar layer of *isotropic* polarizable dipoles in *vacuum*. A similar derivation can be carried out for the two types of anisotropic polarizable dipoles studied in this work (Sec. II B). The dipoles are arranged in a square array with areal density ρ. The dipole plane is the xy plane and we consider incident p-polarized light at an angle θ from the normal (z axis). For perpendicular uniaxial dipoles with polarizability tensor $\underline{\alpha} = \alpha \hat{z} \otimes \hat{z}$, a derivation similar to Ref. [58] results in the following absorption coefficient in vacuum (here given using SI units):

$$A_0^\perp = \frac{k_0 \rho}{\varepsilon_0} \frac{\sin^2 \theta}{\cos \theta} \frac{\mathrm{Im}(\alpha)}{\left| 1 + \frac{\alpha}{4\pi\varepsilon_0} \left[\rho^{3/2} \xi_0 - 2i\pi k_0 \rho \frac{\sin^2\theta}{\cos\theta} \right] \right|^2}, \quad (A1)$$

where $k_0 = 2\pi/\lambda$. The second term in brackets is akin to a radiative correction term [61]. For in-plane dipoles, either uniaxial with random orientation or isotropic in-plane polarizabilities, i.e., $\underline{\alpha} = \alpha[\hat{x} \otimes \hat{x} + \hat{y} \otimes \hat{y}]$, we similarly have

$$A_0^\parallel = \frac{k_0 \rho}{\varepsilon_0} \cos\theta \frac{\mathrm{Im}(\alpha)}{\left| 1 - \frac{\alpha}{4\pi\varepsilon_0} [\rho^{3/2} \xi_0/2 + 2i\pi k_0 \rho \cos\theta] \right|^2}. \quad (A2)$$

For fully isotropic dipoles with $\underline{\alpha} = \alpha\underline{I}$, we simply have $A_0^{\mathrm{iso}} = A_0^\perp + A_0^\parallel$, which is equivalent to Eq. (68) in Ref. [58].

We can generalize these expressions to an embedding medium with dielectric function $\varepsilon_m \neq 1$. Firstly, we assume that the polarizability refers to the microscopic polarizability in vacuum, i.e., the induced microscopic dipole is proportional to the microscopic field: $\mathbf{p} = \underline{\alpha}\mathbf{e}$. The microscopic field is obtained from the macroscopic field by $\mathbf{e} = L_m \mathbf{E}$ where L_m is defined in Eq. (16). By optical reciprocity, the macroscopic field created by this microscopic dipole is also modified by a factor L_m [36,37,56]. In addition, from macroscopic Maxwell's equations [47], the field of a dipole embedded in a continuous medium of dielectric function ε_m is expressed in terms of the medium wave vector $k = 2\pi\sqrt{\varepsilon_m}/\lambda$ instead of k_0 and has a prefactor $1/(4\pi\varepsilon_0\varepsilon_m)$ instead of $1/(4\pi\varepsilon_0)$. Taking all these corrections into account and running through the derivations, we obtain the generalized expressions as

$$A^\perp = \frac{k \rho L_m^2}{\varepsilon_0 \varepsilon_m} \frac{\sin^2 \theta}{\cos \theta} \frac{\mathrm{Im}(\alpha)}{\left| 1 + \frac{\alpha L_m^2}{4\pi\varepsilon_0\varepsilon_m} \left[\rho^{3/2} \xi_0 - 2i\pi k \rho \frac{\sin^2\theta}{\cos\theta} \right] \right|^2}, \quad (A3)$$

$$A^\parallel = \frac{k \rho L_m^2}{\varepsilon_0 \varepsilon_m} \cos\theta \frac{\mathrm{Im}(\alpha)}{\left| 1 - \frac{\alpha L_m^2}{4\pi\varepsilon_0\varepsilon_m} [\rho^{3/2} \xi_0/2 + 2i\pi k \rho \cos\theta] \right|^2}. \quad (A4)$$

The derivations of the effective medium dielectric function (see, e.g., Refs. [40,42]) are very similar to those found in Ref. [58], except that the radiative correction term is absent. The arguments given above can therefore be used to generalize the effective medium dielectric function to an embedding medium with ε_m. We then see from the above arguments that α needs to be corrected by a factor L_m^2/ε_m. Moreover, the relative dielectric function of the embedding medium (which was 1) needs to be replaced by ε_m. These modifications then result
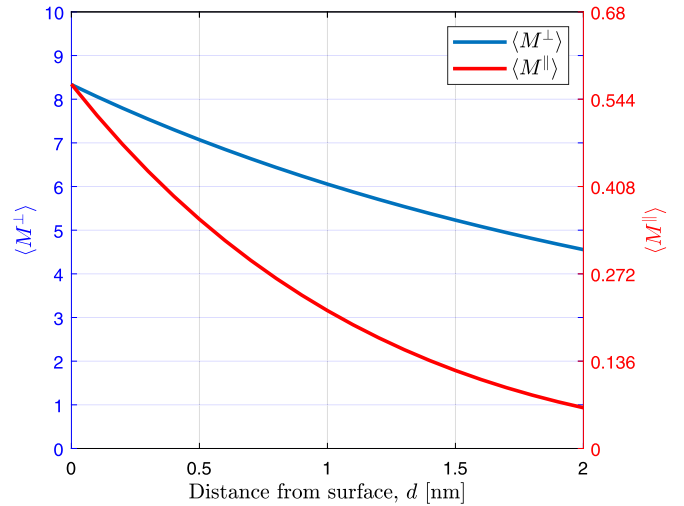
FIG. 7. Surface-averaged field intensity enhancements (perpendicular, left axis, and parallel, right axis, components) at a distance d from a 14-nm-radius silver sphere in water. Note the different scale for the two y axes.

in the proposed expressions for ε_{xy} and ε_z given in the text [Eqs. (13) and (14)].

We note that the radiative correction [second term in the brackets of Eqs. (A3) and (A4)] has only a small influence for coverages up to $\rho \lesssim 1$ nm^{-1}, but it is nevertheless necessary to include it to obtain perfect agreement with the anisotropic EMM predictions (Fig. 3). The EMM dielectric functions [Eqs. (13) and (14)] resemble the expressions above, but interestingly, do not include a radiative correction term. Yet, the EMM predictions do agree with the radiatively corrected expressions above. In this case, retardation effects are accounted for in the solution of Maxwell's equations and do not need to be included in the dielectric function, which only need to account for local interactions.

Finally, we note that implicit in these derivations is the fact that we treat water as a continuum medium in which the dipoles are embedded. This is appropriate in the regime we are interested in, but a different approach may be needed at very high dipole coverages (where water molecules may no longer be dominant in the dipole layer).

APPENDIX B: FIELD ENHANCEMENT AS A FUNCTION OF DISTANCE FROM THE SPHERE

The absorption of a polarizable dipole is proportional to the field intensity at the dipole position. As customary in the context of surface-enhanced spectroscopies [6], we distinguish between the field intensity enhancement factor $\langle M \rangle := \langle |\mathbf{E}|^2/|\mathbf{E_0}|^2 \rangle$ for perpendicular $M^\perp$ and parallel components $M^\parallel$. This can be calculated at different positions outside the sphere and we compute the average enhancements $\langle M \rangle$ for a uniform layer of dipoles at a distance d from the surface of a 14-nm silver sphere. A standard implementation of Mie theory is used [62]. The results are summarized in Fig. 7 at the peak of the resonance for our model dye, $\lambda = 526$ nm. They highlight the fast decrease of $\langle M \rangle$ with d especially for the parallel component. The decrease is also less linear in the
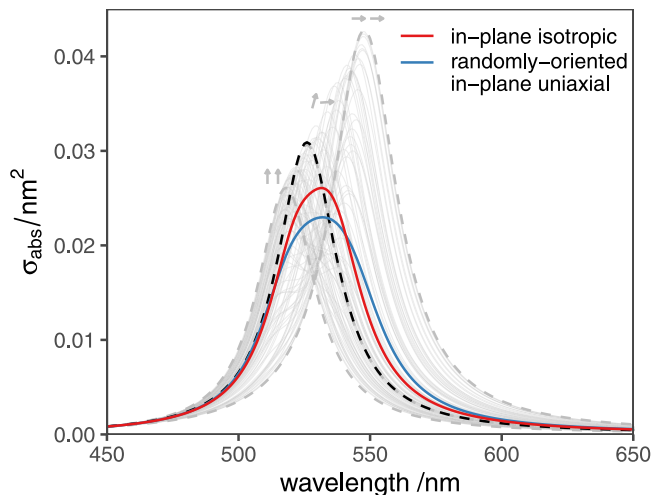
FIG. 8. Simulated absorption spectra for dipolar dimers with separation 0.9 nm. Two types of dipolar polarizabilities are compared: plane-isotropic (red curve), or uniaxial with in-plane random orientation (100 representative light-gray curves are shown). The relative orientation of both dipole moments strongly affects their coupling; the two extreme cases of head-to-tail and side-by-side configurations are presented as dashed gray curves. The average spectrum of any two dipoles randomly oriented in the plane is shown in blue. For reference, the absorption spectrum of a single isolated dye is shown by a black dashed line. All spectra are orientation averaged over all directions of incidence and polarizations.

parallel case, so the average over $0 \leqslant d \leqslant 2$ nm does not correspond to the value at the midpoint $d = 1$ nm.

APPENDIX C: EFFECT OF RELATIVE DIPOLE ORIENTATION

Figure 8 compares the absorption spectrum of a dimer of two in-plane isotropic dipoles to the average spectrum of two uniaxial dipoles with in-plane random orientation. The two configurations are not equivalent, even after averaging (blue vs red curves). This discrepancy occurs because dipole-dipole interactions have a nontrivial dependence on the relative position and orientation of the two dipoles; between the extreme cases of head-to-tail dipoles, leading to a redshift of the absorption spectrum, and side-by-side leading to a blueshift, and a cross configuration (two orthogonal dipoles, leading to no shift of the absorption peak), dipoles in arbitrary orientations will span the full spectral range between these extremes. In contrast the in-plane-isotropic configuration sees the two dipoles always parallel to each other (ignoring minor retardation effects) and with a polarizability reduced by half. This results in a reduction in the range of spectral shifts. A similar conclusion holds for the 3D case, contrasting a dimer with fully isotropic polarizabilities and a dimer with randomly oriented uniaxial dipoles. Here again the random dimer's response does not reduce to that of a dimer of isotropic dipoles, and the average absorption spectrum is broader.

[1] I. S. Maksymov, I. Staude, A. E. Miroshnichenko, and Y. S. Kivshar, Optical Yagi-Uda nanoantennas, Nanophotonics **1**, 65 (2012).

[2] T. Kosako, Y. Kadoya, and H. F. Hofmann, Directional control of light by a nano-optical Yagi-Uda antenna, Nat. Photonics **4**, 312 (2010).

[3] O. Hess, J. B. Pendry, S. A. Maier, R. F. Oulton, J. M. Hamm, and K. L. Tsakmakidis, Active nanoplasmonic metamaterials, Nat. Mater. **11**, 573 (2012).

[4] N. Engheta, Circuits with light at nanoscales: Optical nanocircuits inspired by metamaterials, Science **317**, 1698 (2007).

[5] S. Kühn, U. Håkanson, L. Rogobete, and V. Sandoghdar, Enhancement of Single-Molecule Fluorescence Using a Gold Nanoparticle as an Optical Nanoantenna, Phys. Rev. Lett. **97**, 017402 (2006).

[6] E. C. Le Ru and P. G. Etchegoin, *Principles of Surface-Enhanced Raman Spectroscopy: And Related Plasmonic Effects* (Elsevier, New York, 2009).

[7] C. M. Galloway, P. G. Etchegoin, and E. C. Le Ru, Ultrafast Nonradiative Decay Rates on Metallic Surfaces by Comparing Surface-Enhanced Raman and Fluorescence Signals of Single Molecules, Phys. Rev. Lett. **103**, 063003 (2009).

[8] R. Gill and E. C. Le Ru, Fluorescence enhancement at hotspots: The case of Ag nanoparticle aggregates, Phys. Chem. Chem. Phys **13**, 16366 (2011).

[9] R. Gill, L. Tian, W. R. C. Somerville, E. C. Le Ru, H. van Amerongen, and V. Subramaniam, Silver nanoparticle aggregates as highly efficient plasmonic antennas for fluorescence enhancement, J. Phys. Chem. C **116**, 16687 (2012).

[10] A. Bek, R. Jansen, M. Ringler, S. Mayilo, T. A. Klar, and J. Feldmann, Fluorescence enhancement in hot spots of AFM-designed gold nanoparticle sandwiches, Nano Lett. **8**, 485 (2008).

[11] E. C. Le Ru and P. G. Etchegoin, Single-molecule surface-enhanced Raman spectroscopy, Annu. Rev. Phys. Chem. **63**, 65 (2012).

[12] J. Qi, X. Dang, P. T. Hammond, and A. M. Belcher, Highly efficient plasmon-enhanced dye-sensitized solar cells through metal@oxide core–shell nanostructure, ACS Nano. **5**, 7108 (2011).

[13] O. L. Muskens, J. G. Rivas, R. E. Algra, E. P. Bakkers, and A. Lagendijk, Design of light scattering in nanowire materials for photovoltaic applications, Nano Lett. **8**, 2638 (2008).

[14] W. Ni, T. Ambjornsson, S. P. Apell, H. Chen, and J. Wang, Observing plasmonic–molecular resonance coupling on single gold nanorods, Nano Lett. **10**, 77 (2010).

[15] W. Ni, H. Chen, J. Su, Z. Sun, J. Wang, and H. Wu, Effects of dyes, gold nanocrystals, pH, and metal ions on plasmonic and molecular resonance coupling, J. Am. Chem. Soc. **132**, 4806 (2010).

[16] J. Zhao, L. Jensen, J. Sung, S. Zou, G. C. Schatz, and R. P. Van Duyne, Interaction of plasmon and molecular resonances for rhodamine 6G adsorbed on silver nanoparticles, J. Am. Chem. Soc. **129**, 7647 (2007).

[17] J. Y. Yan, W. Zhang, S. Duan, X. G. Zhao, and A. O. Govorov, Optical properties of coupled metal-semiconductor and metal-molecule nanocrystal complexes: Role of multipole effects, Phys. Rev. B **77**, 165301 (2008).

[18] N. T. Fofang, T. H. Park, O. Neumann, N. A. Mirin, P. Nordlander, and N. J. Halas, Plexcitonic nanoparticles: Plasmon-exciton coupling in nanoshell-J-aggregate complexes, Nano Lett. **8**, 3481 (2008).

[19] T. J. Antosiewicz, S. P. Apell, and T. Shegai, Plasmon-exciton interactions in a core-shell geometry: From enhanced absorption to strong coupling, ACS Photonics **1**, 454 (2014).

[20] A. O. Cacciola, O. Di Stefano, R. Stassi, R. Saija, and S. Savasta, Ultrastrong coupling of plasmons and excitons in a nanoshell, ACS Nano **8**, 11483 (2014).

[21] B. L. Darby, B. Auguié, M. Meyer, A. E. Pantoja, and E. C. Le Ru, Modified optical absorption of molecules on metallic nanoparticles at sub-monolayer coverage, Nat. Photonics **10**, 40 (2016).

[22] A. M. Fales, S. J. Norton, B. M. Crawford, B. G. DeLacy, and T. Vo-Dinh, Fano resonance in a gold nanosphere with a J-aggregate coating, Phys. Chem. Chem. Phys. **17**, 24931 (2015).

[23] R. Chikkaraddy, B. de Nijs, F. Benz, S. J. Barrow, O. A. Scherman, E. Rosta, A. Demetriadou, P. Fox, O. Hess, and J. J. Baumberg, Single-molecule strong coupling at room temperature in plasmonic nanocavities, Nature (London) **535**, 127 (2016).

[24] G. Zengin, T. Gschneidtner, R. Verre, L. Shao, T. J. Antosiewicz, K. Moth-Poulsen, M. Käll, and T. Shegai, Evaluating conditions for strong coupling between nanoparticle plasmons and organic dyes using scattering and absorption spectroscopy, J. Phys. Chem. C **120**, 20588 (2016).

[25] G. P. Wiederrecht, G. A. Wurtz, and J. Hranisavljevic, Coherent coupling of molecular excitons to electronic polarizations of noble metal nanoparticles, Nano Lett. **4**, 2121 (2004).

[26] H. Chen, L. Shao, K. C. Woo, J. Wang, and H. Q. Lin, Plasmonic–molecular resonance coupling: Plasmonic splitting versus energy transfer, J. Phys. Chem. C **116**, 14088 (2012).

[27] G. Zengin, G. Johansson, P. Johansson, T. J. Antosiewicz, M. Käll, and T. Shegai, Approaching the strong coupling limit in single plasmonic nanorods interacting with J-aggregates, Sci. Rep. **3**, 3074 (2013).

[28] A. E. Schlather, N. Large, A. S. Urban, P. Nordlander, and N. J. Halas, Near-field mediated plexcitonic coupling and giant Rabi splitting in individual metallic dimers, Nano Lett. **13**, 3281 (2013).

[29] D. E. Aspnes, Local-field effects and effective medium theory: A microscopic perspective, A. J. Phys. **50**, 704 (1982).

[30] D. E. Aspnes, Optical properties of thin films, Thin Solid Films **89**, 249 (1982).

[31] V. A. Markel, Introduction to the Maxwell Garnett approximation: Tutorial, J. Opt. Soc. Am. A **33**, 1244 (2016).

[32] T. A. R. Purcell, S. Yochelis, Y. Paltiel, and T. Seideman, Determining the molecular dipole orientation on nanoplasmonic structures, J. Phys. Chem. C **122**, 16901 (2018).

[33] V. A. Markel, L. S. Muratov, M. I. Stockman, and T. F. George, Theory and numerical simulation of optical properties of fractal clusters, Phys. Rev. B **43**, 8183 (1991).

[34] E. M. Purcell and C. R. Pennypacker, Scattering and absorption of light by nonspherical dielectric grains, Astrophys. J. **186**, 705 (1973).

[35] M. A. Yurkin and A. G. Hoekstra, The discrete dipole approximation: An overview and recent developments, J. Quant. Spectrosc. Radiat. Transf. **106**, 558 (2007).

[36] B. Auguié and E. C. Le Ru, Optical absorption of dye molecules in a spherical shell geometry, J. Phys. Chem. C **122**, 19110 (2018).

[37] B. Auguié, B. L. Darby, and E. C. Le Ru, Electromagnetic interactions of dye molecules surrounding a nanosphere, Nanoscale **11**, 12177 (2019).

[38] W. R. C. Somerville, B. Auguié, and E. C. Le Ru, Accurate and convergent T-matrix calculations of light scattering by spheroids, J. Quant. Spectrosc. Radiat. Transf. **160**, 29 (2015).

[39] D. Schebarchov, E. C. Le Ru, J. Grand, and B. Auguié, Mind the gap: Testing the Rayleigh hypothesis in T-matrix calculations with adjacent spheroids, Opt. Express **27**, 35750 (2019).

[40] M. J. Dignam and M. Moskovits, Optical properties of sub-monolayer molecular films, J. Chem. Soc., Faraday Trans. 2 **69**, 56 (1973).

[41] A. Bagchi, R. G. Barrera, and B. B. Dasgupta, Classical Local-Field Effect in Reflectance from Adsorbed Overlayers, Phys. Rev. Lett. **44**, 1475 (1980).

[42] A. Bagchi, R. G. Barrera, and R. Fuchs, Local-field effect in optical reflectance from adsorbed overlayers, Phys. Rev. B **25**, 7086 (1982).

[43] J. Roth and M. J. Dignam, Scattering and extinction cross sections for a spherical particle coated with an oriented molecular layer, J. Opt. Soc. Am. **63**, 308 (1973).

[44] C. Tang, B. Auguié, and E. C. Le Ru, Modeling molecular orientation effects in dye-coated nanostructures using a thin-shell approximation of Mie theory for radially anisotropic media, ACS Photonics **5**, 5002 (2018).

[45] A. Djorovic, M. Meyer, B. L. Darby, and E. C. Le Ru, Accurate modeling of the polarizability of dyes for electromagnetic calculations, ACS Omega **2**, 1804 (2017).

[46] D. Schebarchov, B. Auguié, and E. C. Le Ru, Simple accurate approximations for the optical properties of metallic nanospheres and nanoshells, Phys. Chem. Chem. Phys. **15**, 4233 (2013).

[47] J. D. Jackson, *Classical Electrodynamics*, 3rd ed. (Wiley, New York, 2003).

[48] M. Moskovits, Surface selection rules, J. Chem. Phys. **77**, 4408 (1982).

[49] M. Moskovits, Surface-enhanced spectroscopy, Rev. Mod. Phys. **57**, 783 (1985).

[50] E. C. Le Ru, S. A. Meyer, C. Artur, P. G. Etchegoin, J. Grand P. Lang, and F. Maurel, Experimental demonstration of surface selection rules for SERS on flat metallic surfaces, Chem. Commun. **47**, 3903 (2011).

[51] F. H. P. M. Habraken, O. L. J. Gijzeman, and G. A. Bootsma, Ellipsometry of clean surfaces, submonolayer and monolayer films, Surf. Sci. **96**, 482 (1980).

[52] J. Lekner and P. J. Castle, Local fields near the surface of a crystalline dielectric, Physica A (Amsterdam, Neth.) **101**, 89 (1980).

[53] J. Topping and S. Chapman, On the mutual potential energy of a plane network of doublets, Proc. R. Soc. London, Ser. A **114**, 67 (1927).

[54] B. M. E. van der Hoff and G. C. Benson, A method for the evaluation of some lattice sums occurring in calculations of physical properties of crystals, Can. J. Phys. **31**, 1087 (1953).

[55] S. R. Polo and M. K. Wilson, Infrared intensities in liquid and gas phases, J. Chem. Phys. **23**, 2376 (1955).

[56] G. Eckhardt and W. G. Wagner, On the calculation of absolute Raman scattering cross sections from Raman scattering coefficients, J. Mol. Spectrosc. **19**, 407 (1966).

[57] S. Teitler and B. W. Henvis, Refraction in stratified, anisotropic media, J. Opt. Soc. Am. **60**, 830 (1970).

[58] J. Vlieger, Reflection and transmission of light by a square nonpolar lattice, Physica **64**, 63 (1973).

[59] G. W. Ford and W. H. Weber, Electromagnetic interactions of molecules with metal surfaces, Phys. Rep. **113**, 195 (1984).

[60] P. Bharadwaj and L. Novotny, Spectral dependence of single molecule fluorescence enhancement, Opt. Express **15**, 14266 (2007).

[61] E. C. Le Ru, W. R. C. Somerville, and B. Auguié, Radiative correction in approximate treatments of electromagnetic scattering by point and body scatterers, Phys. Rev. A **87**, 012504 (2013).

[62] E. C. Le Ru and P. G. Etchegoin, SERS and plasmonics codes (SPlaC). MATLAB codes freely available from http://www.vuw.ac.nz/raman/book/codes.aspx.